Measurement of bond vector orientations in invisible excited states of proteins

Pramodh Vallurupalli*†‡, D. Flemming Hansen*†‡, Elliott Stollar‡§, Eva Meirovitch¶, and Lewis E. Kay*†‡‖

Departments of *Molecular and Medical Genetics, †Chemistry, and ‡Biochemistry, University of Toronto, Toronto, ON, Canada M5S 1A8; §Molecular Structure and Function, Hospital for Sick Children, Toronto, ON, Canada M5G 1X8; and ¶The Mina and Everard Goodman Faculty of Life Sciences, Bar-Ilan University, Ramat-Gan 52900, Israel

Edited by Adriaan Bax, National Institutes of Health, Bethesda, MD, and approved October 9, 2007 (received for review September 4, 2007)

The focus of structural biology is on studies of the highly populated, ground states of biological molecules; states that are only sparsely and transiently populated are more difficult to probe because they are invisible to most structural methods. Yet, such states can play critical roles in biochemical processes such as ligand binding, enzyme catalysis, and protein folding. A description of these states in terms of structure and dynamics is, therefore, of great importance. Here, we present a method, based on relaxation dispersion NMR spectroscopy of weakly aligned molecules in a magnetic field, that can provide such a description by direct measurement of backbone amide bond vector orientations in transient, low populated states that are not observable directly. Such information, obtained through the measurement of residual dipolar couplings, has until now been restricted to proteins that produce observable spectra. The methodology is applied and validated in a study of the binding of a target peptide to an SH3 domain from the yeast protein Abp1p and subsequently used in an application to protein folding of a mutational variant of the Fyn SH3 domain where ^{1}H-^{15}N dipolar couplings of the invisible unfolded state of the domain are obtained. The approach, which can be used to obtain orientational restraints at other sites in proteins as well, promises to significantly extend the available information necessary for providing a site-specific characterization of structural properties of transient, low populated states that have to this point remained recalcitrant to detailed analysis.

CPMG | dipolar couplings | dynamics | NMR | chemical exchange

Solution NMR spectroscopy is a powerful technique for the study of biomolecular dynamics spanning a range of time scales from picoseconds for bond vector librations to many hours for hydrogen exchange in the buried interiors of proteins (1, 2). One very important approach, based on the concept of a "spin-echo" that was first described by Hahn in 1950 (3), is called the Carr–Purcell–Meiboom–Gill (CPMG) relaxation dispersion method (4, 5). This class of experiment provides a window into processes with conformational exchange on the millisecond time scale (6), a time regime that is often the relevant one for the lifetimes of bound ligands (7, 8), protein folding events (9), or molecular rearrangements that are important for the control of enzyme function (10–13). For systems in which the ground state exchanges with a minor conformer populated at 0.5% or higher and with exchange rates on the order of a hundred to a few thousand per second, the CPMG dispersion experiment provides a sensitive measure of the exchange dynamics (6). Rates of exchange, populations of exchanging states, and chemical shifts of nuclear spins in minor states can be obtained from fits of dispersion profiles to the appropriate model of exchange. Most importantly, information from potentially every residue is obtained in states that are often invisible in even the most sensitive of NMR spectra.

Fig. 1*a* illustrates a simple case in which a loop of a protein, highlighted in green, exchanges between two states for which distinct ^{15}N chemical shifts are obtained (Fig. 1*b*). Typically, the states may have very different populations and lifetimes so that peak intensities are highly skewed, to the point where the minor state is not observed (Fig. 1*b Inset*). The chemical shifts of the invisible excited state can be reconstructed from CPMG relaxation dispersion measurements, where the widths of peaks of the observable state, $R_{2,\mathrm{eff}}$, are measured as a function of the frequency of application of radio-frequency pulses, ν_{CPMG}, that quench the effects of the chemical exchange event(s) (6) [see supporting information (SI) *Text*]. This is possible because the resulting dispersion profiles ($R_{2,\mathrm{eff}}$ vs. ν_{CPMG}) are sensitive to $\Delta\nu$, the difference in chemical shifts between ground and excited states (in hertz). In favorable cases, the derived chemical shifts of the excited state can be interpreted to provide structural information (9). Although exciting developments in using chemical shifts as the sole probes of structure have been forthcoming (14), the relation between chemical shifts and high-resolution structure remains empirical. In solution NMR studies of proteins for which well resolved, high-resolution spectra can be recorded, chemical shifts supplement distance constraints measured from NOE spectra (15), dihedral angle constraints from scalar couplings (16), and orientational restraints in the form of residual dipolar couplings (17, 18) that are combined to generate three-dimensional structures.

Measuring Residual Dipolar Couplings in Invisible States

Residual dipolar couplings are a particularly valuable probe of structure because they relate bond vector orientations in a molecular frame and in this sense provide long-range information that is lacking from other NMR observables (17, 18). In isotropic solution such couplings average exactly to zero, but they can be reintroduced into spectra by dissolving the molecule of interest into a medium that produces weak alignment (18). This leads to peak splittings that can be quantified and related to orientation, so long as the peaks themselves can be observed in spectra. Fig. 1 *c* and *d* illustrates the situation for an amide bond vector attached to a protein dissolved in alignment media. As before, the protein undergoes exchange between major ("A") and minor ("B") conformations; resonance lines for the major and minor states are split into two, with the displacement given by the sum of the scalar coupling, J_{NH}, assumed invariant between conformers, and the dipolar coupling, D_{NH}, that is related to the bond orientation in each state and that in general will be different for corresponding bond vectors in states A and B. In Fig. 1*d*, the spectrum of the minor state is shown (along

Author contributions: P.V. and D.F.H. contributed equally to this work; P.V., D.F.H., E.M., and L.E.K. designed research; P.V., D.F.H., and L.E.K. performed research; P.V., D.F.H., and E.S. contributed new reagents/analytic tools; P.V., D.F.H., and L.E.K. analyzed data; and P.V., D.F.H., and L.E.K. wrote the paper.

The authors declare no conflict of interest.

This article is a PNAS Direct Submission.

‖To whom correspondence should be addressed at: Department of Medical Genetics and Microbiology, 1 King's College Circle, Toronto, ON, Canada M5S 1A8. E-mail: kay@pound.med.utoronto.ca.

This article contains supporting information online at www.pnas.org/cgi/content/full/0708296104/DC1.

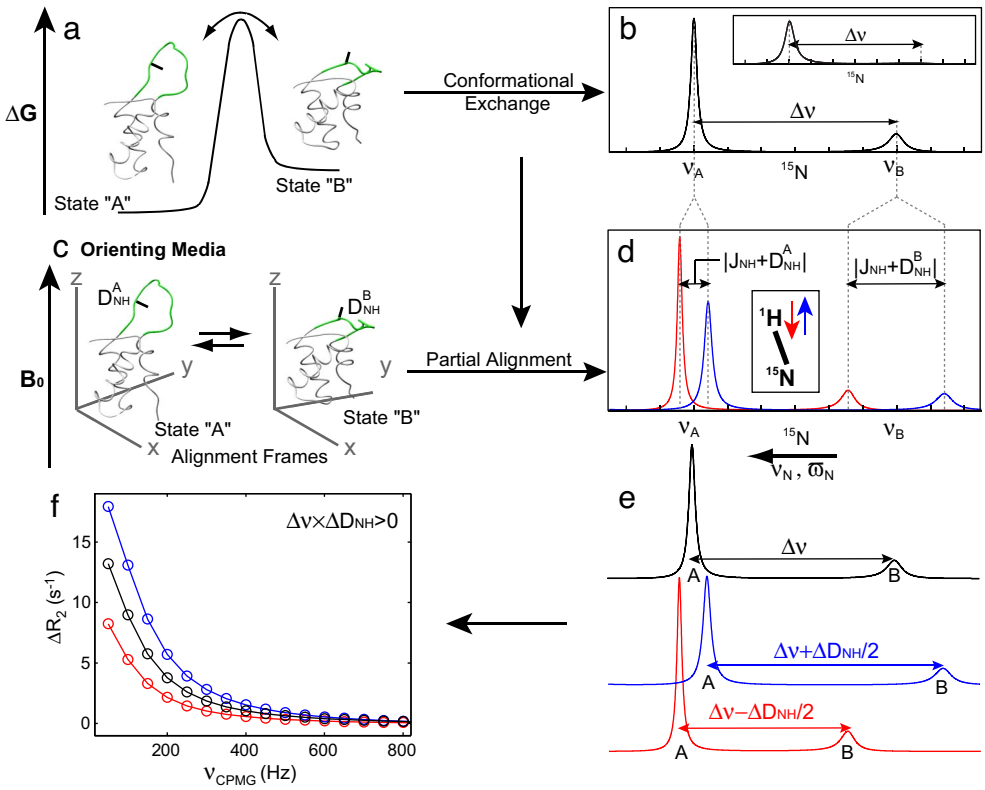

Fig. 1. Measurement of amide bond vector orientation in invisible excited protein states. (*a*) Energy level diagram for a two-state exchanging system, where the loop (green) can exist in two conformations. (*b*) Resulting ^{1}H-decoupled ^{15}N spectrum for a single amide probe of conformational exchange between two states whose populations are highly skewed. In weakly aligning media (*c*) and without ^{1}H decoupling, each line is split by the sum of ^{1}H-^{15}N dipolar and scalar couplings ($J_{NH} \sim -93$ Hz). Spectra resulting from the ^{1}H in the down and up spin-states are shown in *d* in red and blue, respectively. (*e* and *f*) Separate ^{15}N CPMG relaxation dispersion experiments monitor exchange between ground and excited state conformations that are separated by $\Delta\nu$ (black), $\Delta\nu - 0.5\Delta D_{NH}$ (red), or $\Delta\nu + 0.5\Delta D_{NH}$ (blue), from which ΔD_{NH} can be extracted. There is a small contribution to the chemical shift that results from alignment (19) so that ν_A and ν_B are shifted slightly ($\leq$5 Hz for the alignment parameters of the systems considered here at a field of 800 MHz) between *b* and *d* (not included for clarity). Thus, values of $\Delta\nu$ include contributions from incomplete averaging of the anisotropic chemical shift, as described in the text. In *f*, intrinsic relaxation rates, $R_{2,\infty}$, have been subtracted from the dispersion profiles to emphasize their differences, $\Delta R_2 = R_{2,\text{eff}} - R_{2,\infty}$. Note that the relative magnitude of TROSY and anti-TROSY dispersion profiles reverses with the sign of the product $\Delta\nu \times \Delta D_{NH}$.

with the major state) but, in general, will not be observed. Yet, it is still possible to measure dipolar couplings of the "invisible," minor state by using suitably designed CPMG relaxation dispersion experiments. In a "typical" relaxation dispersion NMR experiment, conducted in isotropic solution, exchange is measured between major and minor states that are separated by $\Delta\nu$, and this type of experiment can be performed on fractionally aligned proteins with the appropriate NMR scheme [Fig. 1*e* (black) and SI Fig. 5]. In the case of an aligned system, $\Delta\nu = \Delta\nu_{\text{isotropic}} + \Delta\nu_{\text{anisotropic}}$, where the first term is the isotropic shift difference and the second term arises from the incomplete averaging of the anisotropic chemical shift due to alignment (19). Fig. 1*f* (black) shows the resultant relaxation dispersion profile that derives from the time-dependent modulation of chemical shift by the exchange event(s).

It is also possible to measure conformational exchange in a spin-state selective manner by using amide probes where the ^{15}N spin is coupled to its directly attached ^{1}H in the down (red) or up (blue) spin-state, corresponding to exchange between states separated by $\Delta\nu - 0.5\Delta D_{NH}$ and $\Delta\nu + 0.5\Delta D_{NH}$, respectively, where $\Delta D_{NH} = D_{NH}^{A} - D_{NH}^{B}$ is the difference between ^{1}H-^{15}N dipolar couplings in states A and B, and D_{NH}^{K} is given by an expression in the literature [see equation 3e of Bax *et al.* (20)]. As described above, $\Delta\nu$ consists of contributions from both isotropic and anisotropic interactions, but because the orientation-dependent shift contributions are independent of ^{1}H spin-state, they do not interfere with the extraction of accurate ΔD_{NH} values. Experiments for measuring ΔD_{NH} can be performed in a straightforward way by selecting for TROSY (transverse relaxation optimized spectroscopy; $\Delta\nu - 0.5\Delta D_{NH}$) (21) or anti-TROSY ($\Delta\nu + 0.5\Delta D_{NH}$) magnetization components during CPMG elements in experiments that build on the elegant TROSY-dispersion experiment developed by Palmer and coworkers (22) that is used for measurements in isotropic solution. In the same way that a time-dependent modulation of chemical shift leads to a relaxation dispersion profile (Fig. 1*f*, black), so too can the modulation of dipolar couplings that arises from exchange between states. As expected, dispersion profiles that derive from exchange between states separated by $\Delta\nu \pm 0.5\Delta D_{NH}$ are distinct (Fig. 1*f*, blue and red). Thus, by measuring these three classes of dispersion experiment, all under conditions where the system of interest is weakly aligned, and fitting the data simultaneously, it is possible to extract $|\Delta\nu|$ and $|\Delta\nu \pm 0.5\Delta D_{NH}|$ (dispersion experiments are invariant to the sign of the shift difference). The sign of the dipolar coupling can be resolved, however, by measuring the sign of $\Delta\nu$, achieved by monitoring the variation of peak positions in spectra recorded at different static magnetic field strengths (23).

Fig. 2 shows ^{15}N TROSY- and anti-TROSY-based CPMG relaxation dispersion pulse schemes that have been developed for the quantification of ^{1}H-^{15}N dipolar couplings in invisible states of proteins [details of the experiments are provided in *SI*

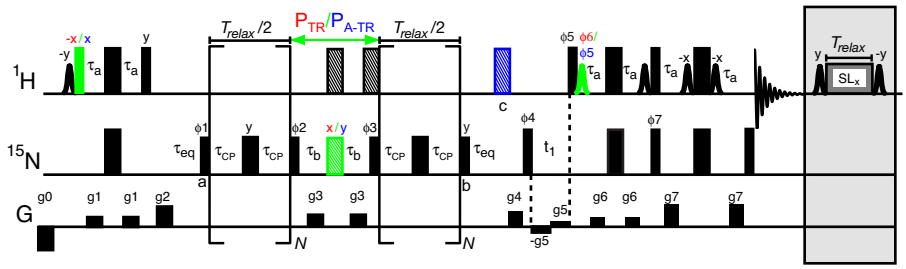

Fig. 2. Pulse schemes of ^{15}N constant-time TROSY and anti-TROSY CPMG relaxation dispersion experiments for measurement of ΔD_{NH} in protein systems undergoing millisecond-time-scale exchange dynamics. All ^{1}H and ^{15}N 90° (180°) radiofrequency pulses are shown as narrow (wide) black bars and are applied at the highest possible power level, with the exception of the ^{15}N refocusing pulses of the CPMG element, along with the 90° sandwiching pulses, which are applied at a slightly lower power level (≈6 kHz). Composite 180° pulses (34) are represented by "striped" rectangles. All pulse phases are assumed to be *x*, unless indicated otherwise. *N* can be any integer. Differences in the TROSY/anti-TROSY schemes are highlighted (in red and blue for TROSY and anti-TROSY, respectively; the 180° pulse at point *c* is omitted in the case of the TROSY experiment). Water-selective 90° ^{1}H pulses (shaped pulses) are rectangular (≈1.6 ms). The phase cycling used is as follows (Varian): $\phi1 = \{x, -x\}$; $\phi2 = 2\{y\}, 2\{-y\}$; $\phi3 = 2\{x\}, 2\{-x\}$; $\phi4 = 2\{y\}, 2\{-y\}, 2\{-x\}, 2\{x\}$; $\phi5 = -y$; $\phi6 = y$; $\phi7 = -y$; receiver = $\{y, -y, -y, y, x, -x, -x, x\}$. Sensitivity enhanced quadrature detection in the indirect dimension (35–38) is obtained by recording a second data set with $\phi4 = 2\{y\}, 2\{-y\}, 2\{x\}, 2\{-x\}$; $\phi5 = \phi5 + \pi$; $\phi6 = \phi6 + \pi$; $\phi7 = \phi7 + \pi$; and receiver = receiver + π for each t_1 increment. In addition, phase $\phi4$ is incremented along with the receiver by 180° for each complex t_1 point (39). The delays used are $\tau_a = 2.25$ ms, $\tau_b = 1/(4|J_{NH}|) = 2.68$ ms, and $\tau_{eq} = (2 - 3)/(k_{ex}) \sim 5$ ms. Gradient strengths G/cm (length in milliseconds) are as follows: g0 = −15(1), g1 = 5(1), g2 = 12(1), g3 = 8(0.3), g4 = 10(0.5), g5 = 0.5(t_1), g6 = 6(0.3), g7 = 25(0.3). A spin-lock element is applied immediately after acquisition at the same power level and for the same duration (T_{relax}) as used for the experiment measuring $|\Delta\nu|$ (SI Fig. 5) so that the heating effects are constant over all measurements.

Text, along with a dispersion experiment for measuring $|\Delta\nu|$ (SI Fig. 5)]. Central to the dispersion experiments is the constant-time CPMG pulse train of duration T_{relax}. In the case of the TROSY scheme, only the TROSY components that are present during the CPMG element are selected and recorded during (t_1, t_2). In contrast, in the anti-TROSY scheme a ^{1}H 180° pulse is inserted at point *c* that interconverts TROSY and anti-TROSY magnetization components, with the TROSY components subsequently selected. Thus, cross-peaks in "anti-TROSY" spectra are of the TROSY variety but report on exchange between anti-TROSY components during the CPMG pulse element. This leads to clear improvements in resolution and sensitivity over schemes that maintain the anti-TROSY components throughout.

To extract accurate ΔD_{NH} values, exchange between TROSY and anti-TROSY components must be minimized during the CPMG relaxation element of Fig. 2 (see *SI Text*). In the case of a ^{1}H-^{15}N spin pair, such exchange results from relaxation of the ^{1}H spin with external protons that effectively "flip" the spin-state of the ^{1}H of interest (Fig. 1*d*, red and blue arrows). Such spin-flips can be minimized effectively through the use of highly deuterated proteins and applications described here have used such deuterated systems. In addition, the small ^{1}H spin-flip rate has been quantified on a per-residue basis (as described under *Data Analysis* in *SI Text*) and subsequently used in fits of TROSY and anti-TROSY relaxation dispersion profiles to account for relaxation from external protons (software available from the authors upon request).

Applications of the Methodology

As a first example that serves to establish the validity of the methodology, we have studied the binding of a 17-residue target peptide from the protein Ark1p to the SH3 domain from Abp1p (24) ($K_d = 0.55 \pm 0.05$ μM; data not shown). In these studies, binding was monitored through the SH3 domain that was ^{15}N-labeled. Large relaxation dispersion profiles were obtained in measurements performed on protein dissolved in isotropic solution (no alignment media) when a small amount of Ark1p peptide was added ([Ark1p]/[SH3] ~ 5%). The chemical-shift differences extracted from fits of relaxation dispersion profiles to a simple two-site exchange model,

$$P + L \underset{k_{off}}{\overset{k_{on}}{\rightleftharpoons}} PL,$$

produced $\Delta\nu$ values that are in excellent agreement with chemical-shift differences between free and fully bound SH3 domain that have been measured directly from separate protein samples (SI Fig. 6). Values of $k_{on} = (6.3 \pm 0.7) \times 10^8$ M^{-1}·s^{-1} and $k_{off} = 350 \pm 10$ s^{-1} were calculated from the dispersion data recorded at 25°C with the larger than diffusion limited k_{on} reflecting the large contribution from electrostatics to binding (the Abp1p SH3 domain has a net negative charge of 12 and the Ark1p peptide a net positive charge of 6 at pH 7).

Fig. 3*a* shows regions of ^{1}H, ^{15}N correlation spectra of the Abp1p SH3 domain with 6.8% and 100% bound peptide (25°C). Peak positions in the spectrum of the 6.8% sample are essentially identical to those in spectra of the apo-state with significant differences in comparison to the fully bound spectrum (SI Fig. 7). Correlations from the minor state, corresponding to the bound form in the 6.8% sample, are not observed in spectra because of severe exchange broadening and the low population of the bound conformer. It is therefore not possible to measure dipolar couplings of this state by using standard experiments. The significant change in the charge of the complex relative to that of the free SH3 domain suggests, however, that there will be large changes in molecular alignment for bound and free protein dissolved in a charged, weakly ordering medium, such as the phage particles used for alignment here (SI Fig. 8). Thus, for protein dissolved in ordering media, the exchange reaction will lead to a time-dependent modulation of alignment and hence of bond vector orientations relative to the external magnetic field. Dipolar couplings can therefore be quantified by using the experiments described above. In principle, modulation of dipolar couplings could also occur through structural changes that accompany ligand binding. However, recent studies have shown that such structural changes are minimal for the Abp1p SH3 domain (unpublished data).

Fig. 3 *b–d* shows TROSY and anti-TROSY relaxation dispersion profiles for select residues from Abp1p SH3 with 6.8% bound peptide, measured on a fractionally aligned sample. In the absence of alignment, TROSY and anti-TROSY dispersions are equivalent to within noise (see below), but differences can manifest for partially oriented samples. Cases where $\Delta\varpi$ (shift differences in parts per million) and ΔD_{NH} have the same (Tyr-8) and opposite (Leu-49) signs are presented, along with an example where $\Delta D_{NH} \sim 0$ for which TROSY and anti-TROSY profiles are similar (Asp-35).

Dispersion profiles were analyzed simultaneously to extract common exchange rates and populations, along with values of

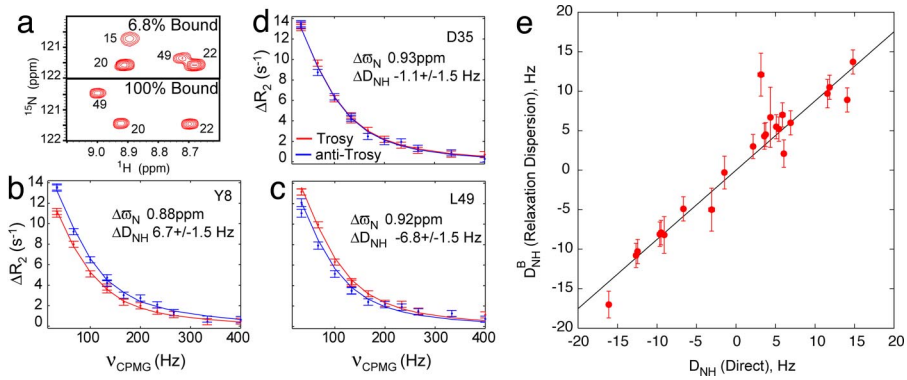

Fig. 3. Measuring ^{1}H-^{15}N dipolar couplings of the invisible peptide-bound state of the Abp1p SH3 domain and validation of the methodology. (*a*) Selected region of ^{1}H-^{15}N TROSY-HSQC spectra of Abp1p SH3 with 6.8% and 100% peptide bound, 800 MHz, 25°C. (*b–d*) Dispersion profiles of selected residues measured at 800 MHz, from which ΔD_{NH} is obtained (as described in the text). Intrinsic relaxation rates have been subtracted from the dispersion curves. (*e*) Dipolar couplings of the invisible minor state, corresponding to the Ark1p peptide-bound form of Abp1p SH3, D^B_{NH}, agree well with dipolar couplings, D_{NH}, measured directly from a fully bound sample. As couplings from separate samples are compared with small differences in the amounts of phage and hence slight differences in A_a values, the slope of the best-fit correlation is not 1 [$(A_a, R) = ((-6.4 \pm 0.3) \times 10^{-4}, 0.38 \pm 0.07)$ and $((-7.35 \pm 0.05) \times 10^{-4}, 0.36 \pm 0.01)$ calculated from D^B_{NH} and D_{NH}, respectively]. Alignment parameters A_a and R are as defined in ref. 18.

$\Delta\varpi$ and ΔD_{NH} for each residue. To obtain dipolar couplings of the minor, invisible state (bound), D^B_{NH}, dipolar couplings of the ground state (apo), D^A_{NH}, were measured directly (on the same sample) by using conventional experiments (25) and subtracted from ΔD_{NH}. Values of D^B_{NH} in this case can be verified by a comparison with corresponding D_{NH} values that are measured directly from spectra of the fully bound form. Fig. 3*e* shows a correlation plot of such a comparison and it is clear that very good agreement is obtained, verifying the methodology (SI Tables 1 and 2). Of interest, the one significant outlier in the plot is Asp-15, which has a ^{1}H spin-flip rate that is 3-fold higher than for all other amides. In principle, this outlier could easily be eliminated on the basis of its anomalous relaxation properties, although we have not done so here. As a further verification, we calculated the orientation of alignment tensors determined from the structure of the Ark1p peptide/Abp1p SH3 complex using either (*i*) D^B_{NH} values measured by means of relaxation dispersion on the 6.8% bound sample where correlations from the complex are "invisible" or (*ii*) D_{NH} values measured directly from spectra of the fully bound state, and each of the corresponding principal axes of the two frames is within 6° (SI Fig. 8 and SI Table 1).

As a second example demonstrating the approach, the folding reaction of the G48M Fyn SH3 domain (9) is considered. Previous relaxation dispersion studies (26) (without alignment) have shown that the folding reaction proceeds from an invisible unfolded state populated at 5% ($p_U = 5\%$) through an on-pathway intermediate populated at 0.7% that is also not observed in spectra. Because p_I is close to an order of magnitude smaller than p_U, the reaction can be approximated as two-state to first-order, as indicated in SI Fig. 9, which shows a good correlation between shifts of the unfolded, excited state extracted from the two-state model and predicted random coil values. In the isotropic phase, TROSY and anti-TROSY dispersion profiles are identical (Fig. 4*a*) but become very different in the aligned sample (Fig. 4*b*), which reflects the nonzero values of ΔD_{NH}. Dipolar couplings of the ground (green, folded) and excited (red, unfolded) states are shown in Fig. 4*c* (SI Table 3), and as expected the dipolar couplings from the unfolded state are significantly attenuated relative to those from the folded domain because of an increased level of dynamics. Further analysis of the dipolar couplings of the unfolded state in terms of structural preferences of the ensemble must await additional experiments, performed by using alignment media where electrostatic contributions to alignment are significantly reduced over their effects here, simplifying the interpretation of the data (because steric effects only can then be used to predict the alignment properties of the ensemble).

As described in *Material and Methods* and *SI Text*, dipolar couplings from residues whose dispersion profiles were fit with reduced $\chi^2 > 2$ or where $\Delta\varpi < 0.2$ ppm were removed from Fig. 4*c* (and Fig. 3*e*). In practice, when $|\Delta\varpi|$ values are below a certain threshold (0.2 ppm used here), it is not possible to extract accurate values of ΔD_{NH} because dispersion profiles are small. In

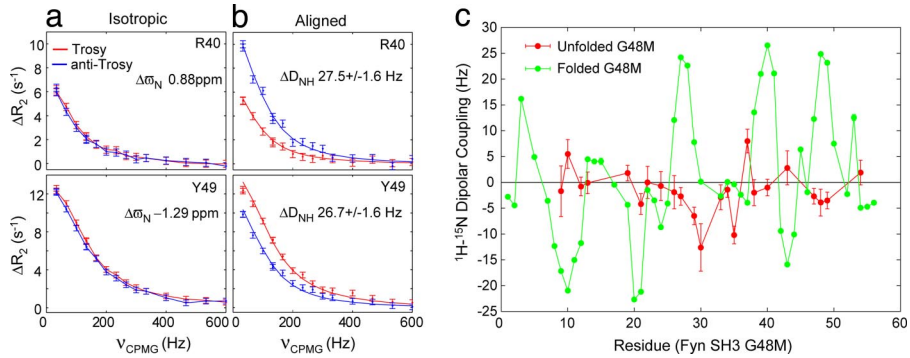

Fig. 4. Measuring ^{1}H-^{15}N dipolar couplings of the excited, unfolded state of the G48M Fyn SH3 domain. (*a*) TROSY and anti-TROSY ^{15}N dispersion profiles (800 MHz) are identical when measured in isotropic phase, with clear differences when protein is dissolved in aligning media (*b*). (*c*) Comparison of D^B_{NH} (red) and D^A_{NH} (green) values of the invisible unfolded state and the folded conformer measured on the same sample by means of relaxation dispersion and direct methods, respectively.

principle, nonflat dispersion curves, even for $\Delta\varpi \approx 0$ ppm, can be obtained in cases where $\Delta D_{NH} \neq 0$; however, in the applications considered presently, the degree of alignment was not sufficient to produce quantifiable dispersion profiles in these cases. The folding example presented here is particularly challenging because many residues have large $\Delta\varpi$ (see SI Table 3) that tend to "mask" ΔD_{NH} values. SI Fig. 10 shows that the error in extracted ΔD_{NH} increases rapidly with $\Delta\varpi$ for shift differences >5 ppm. Remarkably, however, it is possible to extract D^{B}_{NH} values that are well under 10% of $|\Delta\nu \pm 0.5\Delta D_{NH}|$, despite linewidths of peaks from the invisible state that are >100 Hz. This results directly from the fact that dispersion profiles reporting on $\Delta\nu + 0.5\Delta D_{NH}$, $\Delta\nu$, and $\Delta\nu - 0.5\Delta D_{NH}$ can be obtained.

In summary, a method is presented for the measurement of dipolar couplings of low populated, transient states that are "invisible" in NMR spectra. The method relies on the fact that modulation of both chemical shifts and dipolar couplings occurs in exchanging systems that are partially aligned. It is thus possible to measure both chemical shifts and bond vector orientations of excited protein states that can be used as a basis for the calculation of structures, expanding along the lines described in ref. 9. In studies of unfolded proteins, the extracted dipolar couplings can be used to test assumptions of structural preferences of the ensemble, as has recently been demonstrated in applications to the nucleocapsid-binding domain of the Sendai virus (27) and α-synuclein (28, 29). It now becomes possible, however, to carry out studies on systems where such unfolded states are not the predominant forms in solution, without increasing their concentration through the addition of denaturants that could perturb structure or lead to aggregation (30). Further applications of interest include studies of ligand binding to occluded sites in receptors where it is clear that entry must occur through structural rearrangements that are only transiently sampled (7) or studies of enzymes where function involves loop rearrangements (10, 11, 31). In the later case, little may be known about the "excited" loop conformations, and dipolar couplings provide a powerful way to probe them. It is becoming increasingly clear that excited states play an important role in biochemical processes; the methodology presented here provides tools for their characterization at a level of detail that has normally been reserved for applications to highly populated conformations.

Materials and Methods

Sample Preparation. The Abp1p and G48M Fyn SH3 domains, along with the Ark1p peptide, were expressed and purified as described in *SI Text*. The Abp1p/Ark1p sample was ≈90% U-^{2}H, ≈100% U-^{15}N-labeled, 1.3 mM in protein, 6.8% bound peptide, 50 mM sodium phosphate, 100 mM NaCl, 1 mM EDTA, 1 mM NaN_3, 90%/10% H_2O/D_2O, pH 7.0. The G48M Fyn SH3 domain sample was ≈98% U-^{2}H, ≈100% U-^{15}N-labeled, 1 mM in protein, 50 mM sodium phosphate, 1 mM EDTA, 1 mM NaN_3, 90%/10% H_2O/D_2O, pH 7.0. Sample alignment was obtained through the addition of ≈25 mg/ml (Abp1p SH3) and ≈35 mg/ml (G48M Fyn SH3) Pf1 phage (32), purchased from ASLA BIOTECH (residual ^{2}H water splitting of ≈30 Hz), which provided dipolar couplings between −10 and +7 Hz and −22 and +26 Hz for the Abp1p (apo) and Fyn (folded) SH3 domains, respectively.

NMR Spectroscopy and Data Analysis. A set of constant-time ^{15}N CPMG relaxation dispersion experiments (TROSY, anti-TROSY, and ^{1}H CW decoupled) were recorded on fractionally aligned samples (25°C) at a pair of static magnetic field strengths corresponding to ^{1}H resonance frequencies of 500 and 800 MHz, using spectrometers equipped with room-temperature probeheads. Experimental details are given in *SI Text*. Residual dipolar couplings of major state (observable) conformations were measured by using the IPAP approach (25).

Datasets were processed and analyzed with the program NMRPipe (33), and signal intensities were quantified by using the program FuDA (available upon request). Relaxation dispersion data were interpreted by using a two-state exchange model described in *SI Text*, with all dispersions analyzed simultaneously. Dipolar couplings from residues whose dispersion profiles were fit with reduced $\chi^2 > 2$ or where $\Delta\varpi < 0.2$ ppm were removed from Figs. 3*e* and 4*c* but are included in SI Tables 2 and 3. Also removed from Fig. 4*c* are points for which errors in D^{B}_{NH} values exceed the range of experimental D^{B}_{NH} couplings (±5 Hz; see SI Fig. 10).

We thank Dr. Julie Forman-Kay, Dr. Dmitry Korzhnev, Dr. Philipp Neudecker, Dr. Ranjith Muhandiram, and Ms. Hong Lin for useful discussions. This work was supported by grants from the Canadian Institutes of Health Research (to L.E.K.) and the Israel Science Foundation (Grant 279/03 to E.M.). D.F.H. is the recipient of a postdoctoral fellowship from the Danish Agency for Science, Technology, and Innovation (No. 272-05-0232). P.V. and E.S. have postdoctoral fellowships from a Canadian Institutes of Health Research Training Grant on Protein Folding in Health and Disease. L.E.K. holds a Canada Research Chair in Biochemistry.

1. Palmer AG, Williams J, McDermott A (1996) *J Phys Chem* 100:13293–13310.
2. Ishima R, Torchia DA (2000) *Nat Struct Biol* 7:740–743.
3. Hahn EL (1950) *Phys Rev* 80:580–594.
4. Carr HY, Purcell EM (1954) *Phys Rev* 4:630–638.
5. Meiboom S, Gill D (1958) *Rev Sci Instrum* 29:688–691.
6. Palmer AG, Kroenke CD, Loria JP (2001) *Methods Enzymol* 339:204–238.
7. Mulder FAA, Mittermaier A, Hon B, Dahlquist FW, Kay LE (2001) *Nat Struct Biol* 8:932–935.
8. Sugase K, Dyson HJ, Wright PE (2007) *Nature* 447:1021–1024.
9. Korzhnev DM, Salvatella X, Vendruscolo M, Di Nardo AA, Davidson AR, Dobson CM, Kay LE (2004) *Nature* 430:586–590.
10. Wolf-Watz M, Thai V, Henzler-Wildman K, Hadjipavlou G, Eisenmesser EZ, Kern D (2004) *Nat Struct Mol Biol* 11:945–949.
11. Kovrigin EL, Loria JP (2006) *Biochemistry* 45:2636–2647.
12. Eisenmesser EZ, Millet O, Labeikovsky W, Korzhnev DM, Wolf-Watz M, Bosco DA, Skalicky JJ, Kay LE, Kern D (2005) *Nature* 438:117–121.
13. Boehr DD, McElheny D, Dyson HJ, Wright PE (2006) *Science* 313:1638–1642.
14. Cavalli A, Salvatella X, Dobson CM, Vendruscolo M (2007) *Proc Natl Acad Sci USA* 104:9615–9620.
15. Wüthrich K (1986) *NMR of Proteins and Nucleic Acids* (Wiley, New York).
16. Bax A, Vuister GW, Grzesiek S, Delaglio F, Wang AC, Tschudin R, Zhu G (1994) *Methods Enzymol* 239:79–105.
17. Tolman JR, Flanagan JM, Kennedy MA, Prestegard JH (1995) *Proc Natl Acad Sci USA* 92:9279–9283.
18. Tjandra N, Bax A (1997) *Science* 278:1111–1114.
19. Cornilescu G, Bax A (2000) *J Am Chem Soc* 122:10143–10154.
20. Bax A, Kontaxis G, Tjandra N (2001) *Methods Enzymol* 339:127–174.
21. Pervushin K, Riek R, Wider G, Wüthrich K (1997) *Proc Natl Acad Sci USA* 94:12366–12371.
22. Loria JP, Rance M, Palmer AG (1999) *J Biomol NMR* 15:151–155.
23. Skrynnikov NR, Dahlquist FW, Kay LE (2002) *J Am Chem Soc* 124:12352–12360.
24. Haynes J, Garcia B, Stollar EJ, Rath A, Andrews BJ, Davidson AR (2007) *Genetics* 176:193–208.
25. Ottiger M, Delaglio F, Bax A (1998) *J Magn Reson* 131:373–378.
26. Korzhnev DM, Neudecker P, Mittermaier A, Orekhov VY, Kay LE (2005) *J Am Chem Soc* 127:15602–15611.
27. Bernado P, Blanchard L, Timmins P, Marion D, Ruigrok RW, Blackledge M (2005) *Proc Natl Acad Sci USA* 102:17002–17007.
28. Bernado P, Bertoncini CW, Griesinger C, Zweckstetter M, Blackledge M (2005) *J Am Chem Soc* 127:17968–17969.
29. Bertoncini CW, Jung YS, Fernandez CO, Hoyer W, Griesinger C, Jovin TM, Zweckstetter M (2005) *Proc Natl Acad Sci USA* 102:1430–1435.
30. Zhang O, Forman-Kay J (1997) *Biochemistry* 36:3959–3970.
31. Williams JC, McDermott AE (1995) *Biochemistry* 34:8309–8319.
32. Hansen MR, Mueller L, Pardi A (1998) *Nat Struct Biol* 5:1065–1074.
33. Delaglio F, Grzesiek S, Vuister GW, Zhu G, Pfeifer J, Bax A (1995) *J Biomol NMR* 6:277–293.
34. Levitt M, Freeman R (1978) *J Magn Reson* 33:473–476.
35. Kay LE, Keifer P, Saarinen T (1992) *J Am Chem Soc* 114:10663–10665.
36. Schleucher J, Sattler M, Griesinger C (1993) *Angew Chem Int Ed Engl* 32:1489–1491.
37. Pervushin KV, Wider G, Wüthrich K (1998) *J Biomol NMR* 12:345–348.
38. Loria JP, Rance M, Palmer AG (1999) *J Magn Reson* 141:180–184.
39. Marion D, Ikura M, Tschudin R, Bax A (1989) *J Magn Reson* 85:393–399.